Journal of Membrane Science and Research 5 (2019) 274-282

Journal of Membrane Science & Research

journal homepage: www.msrjournal.com

Research Paper

Combined Three Mechanisms Models for Membrane Fouling during Microfiltration

Hamed Koonani, Mehdi Amirinejad *

Membrane Research Center, Faculty of Petroleum and Chemical Engineering, Razi University, Kermanshah, Iran

Article info

Received 2018-10-16
Revised 2019-03-28
Accepted 2019-03-28
Available online 2019-03-28

Keywords

Microfiltration
Fouling
BSA
Triple Models
Blocking

Highlights

- Microfiltration of BSA by three mechanisms models for membrane fouling
- Combination of classical models using the Hagen–Poiseuille law
- Zero-order standard, complete pore blockage and cake formation model
- Zero-order standard, intermediate pore blockage and cake formation model

Graphical abstract

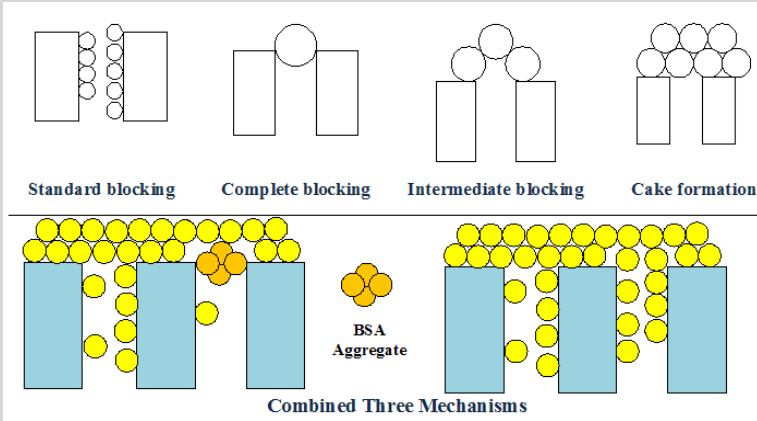

Abstract

Five new mathematical triple fouling models were developed to explore the flux decline behavior during the microfiltration. The first model was developed by the assumption of the successive effects of standard mechanism, intermediate pore blockage and cake formation by using the standard blocking flux expression in the model calculations. The second and third models also obtained by the successive effects of pore constriction, pore blockage and cake formation mechanisms but in the calculation of these models, the Hagen-Poisseuille law for the filtrate flux has been used. For the fourth and fifth models, the classical standard mechanism has been modified by the assumption of zero order time dependent equation for the particle deposition inside the pores. In these models, the zero-order standard mechanism has been used instead of the classical standard mechanism to combine with the pore blockage and then the cake formation mechanism and the Hagen-Poisseuille law. The ability of developed models for the prediction of experimental data for the bovine serum albumin (BSA) filtration was examined. The zero-order standard complete pore blockage-cake formation and the zero-order standard intermediate pore blockage-cake formation models provide fit experimental data, and predict well.

1. Introduction

The main drawback of the membrane-based separation processes is the reduction in the permeate flux during the filtration. Scrutinizing and analyzing the fouling phenomenon and discover the ways to minimize or postpone this phenomenon is very important in the membrane processes. Membrane fouling may occur due to concentration polarization development over the membrane surface, formation of a cake layer or membrane pore blocking. Pore blocking is classified as complete, intermediate and standard pore blocking [1].

In previous studies, some research groups [2-4] have considered only one of the classical fouling mechanisms as the dominant mechanism throughout the filtration. Recent studies [5-7] demonstrated that the blocking models might change from one to another during the microfiltration (MF). For example, Bolton et al. [8] proposed five new double models combining two individual fouling mechanisms. Pore blockage and cake filtration models have also been proposed to describe the cross-flow filtration process with some modifications. Hwang and Lin [6] showed that the blocking models have been changed to the cake filtration model after a period of time for MF-Millipore, Durapore and Isopore membranes. Tracey and Davis [9] examined the membrane total resistance versus the time for the bovine serum albumin (BSA) solution filtration and found that the data in the initial period is consistent with the pore blockage mechanism while the cake model is dominant in the long times. Therefore, a single simple model may not be enough to give good estimation for the permeate flux in the filtration process. Ho and Zydney [10] used the combined models including the pore blockage followed by the cake filtration model for the fouling of protein filtration. Their membrane resistance was increased in the initial by the pore blockage and subsequent fouling was due to the growth of the protein cake layer deposited on these blocked regions. Ho and Zydney's model has been used by other researchers [11, 12]. The impression of internal fouling was conniving

* Corresponding author at: Phone: +98 83 34343342; fax: +98 83 34343321
E-mail address: amirinejad@razi.ac.ir (M. Amirinejad)

DOI: 10.22079/jmsr.2019.95781.1224

in these combined models.

Internal fouling caused by the protein adsorption in the complicated membrane structure may be important for the cases which the feed stream has a relatively low concentration of foulant. For example, Taniguchi et al. [12] reported some irreversible internal fouling models using low molecular weight species. Cassano et al. [13] observed that the standard pore blocking governed the flux decline at low Reynolds number, while the complete pore blocking was significant at the higher Reynolds number. Therefore, it is warranted to develop combined sequential models consisting of internal and external fouling. Orsello et al. [14] proposed triple mechanism models to describe the flux decline during stirred batch ultrafiltration of protein solution.

Nakamura and Matsumoto [15] investigated the fouling mechanism during the dead-end microfiltration of BSA with porous glass membrane. They considered the BSA adsorption onto the pore surface of membrane under the condition of pH 5.0 and ionic strength 0.01. They found that the adsorption rate was proportional to the feed rate of BSA and proportional coefficient. Bowen et al. [16] studied the flux decline experimentally with the dead-end microfiltration of BSA solutions (1 and 0.1 kg/m^3) through Cyclopore track-etched polycarbonate membranes (pore sizes 0.1, 0.2, 0,4 and 1.0 μm) at pH 5 and with NaC1 0.01 M. Their experimental results are examined by successive or simultaneous steps of the flux decline. Xiao et al. [17] investigated the combined effect of the used membrane and the foulant hydrophobicity as well as the surface charge on adsorptive fouling during the microfiltration. Jacob et al. [18] analyzed the structural modifications associated with the fouling kinetics and dynamical changes on the structure of four microporous membranes when fouled by permeating a protein aqueous solution BSA at 1 g/L under 10 kPa in a dead-end device. They obtained the structure after different fouling times by using an extended bubble point method, and the equilibrium (BSA at both 1 and 10 g/L concentrations) and dynamical adsorption, along with the equivalent number of layers. Ye et al. [19] carried out a dead end unstirred filtration of sodium alginate (a model of polysaccharide) and analyzed data using classic filtration laws and the combined pore blockage and cake formation model. They found that the cake model appears to fit the entire range of the ultrafiltration data while the consecutive standard pore blocking model and cake model were more applicable to microfiltration membranes (0.2 μm track-etched and 0.22 μm PVDF membranes). Hou et al. [20] proposed the steady membrane frontal area (K) to improve the predictive accuracy of cake-complete model for combined fouling mechanisms of complete blocking and cake filtration. Their results showed that the predictions of the proposed model had good agreements with experimental data under different conditions for BSA solution. The larger K value was obtained at higher concentration and lower pressure which represented less fouling caused by the complete blocking. Recently, the membrane fouling for binary system including protein and polysaccharides feed has been investigated [21-24]. The related examples are BSA/humic acid, BSA/dextran, BSA/lysozyme and of BSA/pepsin.

The classical models are based on the assumption that the classic mechanism is only effective mechanism. On the other hand, the interaction of each mechanism has been ignored. For example, internal fouling has been considered by the assumption that all particles contribute in internal fouling and then its equation was used to develop combined models of fouling. But in real condition, some portion of particles may contribute to the internal fouling and some else may supply to the pore blockage or cake filtration.

In this study, five triple mechanism models were developed to describe better the flux decline during BSA solutions filtration in the concentration range from 1 to 8 g/L. In all of these models, the mechanisms occur sequentially as internal fouling followed by external fouling. For development of the first model, the standard pore blocking, intermediate pore blocking and cake filtration were combined according to Orsello et al. [14]. Second and third models also obtained by sequential effects of the pore constriction, pore blockage and cake formation mechanisms similar to Orsello and co-workers, but the Hagen-Poisseuille law was considered for calculating these two models. For development of two other models, the classical equations of internal fouling were modified, and combined with the modified standard pore blockage mechanism (zero order pore constriction equation) and they then combined with one of the classical pore blockage mechanisms (complete pore blocking or intermediate pore blocking) and cake formation mechanism. For validation of the models prediction, microfiltration of BSA was tested and the volumetric flow rate was measured versus the time. For every model, the some square error (SSE) was measured to evaluate the consistency of the models with the experimental data.

2. Classical models

The classical models that only consider one mechanism include standard blocking, complete blocking, intermediate blocking and cake filtration. The schematic representation for theses classical models is found in Figure 1-a. In standard blocking, particles enter through the pores and pore constriction is occurred. In cake filtration, the surface particle deposit is formed. The physical concept of the intermediate blocking is the simultaneous occurrence of pore blocking and surface deposit. The method for obtaining the relations for definition of these models can be found in [8]. In summary, the relations for the total filtrate volume per area (V) versus initial filtrate flux of clean membrane (J_0), their constant parameters (K_s, K_b, K_i and K_c) and the time (t) are as follows:

$$V = \left(\frac{1}{J_0 t} + \frac{K_s}{2}\right)^{-1} \quad (1)$$

$$V = \frac{J_0}{K_b}\left(1 - exp(-K_b t)\right) \quad (2)$$

$$V = \frac{1}{K_i} ln(1 + K_i J_0 t) \quad (3)$$

$$V = \frac{1}{K_c J_0}\left(\sqrt{1 + 2K_c J_0^2 t} - 1\right) \quad (4)$$

Eqs. (1), (2), (3) and (4) show the total filtrate volume for the standard blocking, the complete blocking, the intermediate blocking and the cake filtration, respectively.

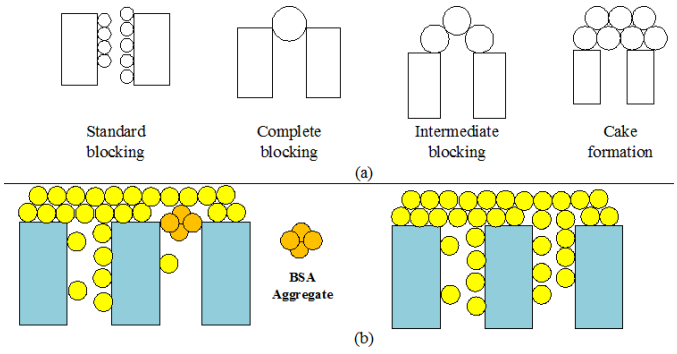

Fig. 1. Schematic representation of (a) classical models, and (b) combined mechanism models; Left: standard complete cake filtration (SCC); Right: standard intermediate cake filtration (SIC).

3. Development of combined three mechanisms models

In this study, fouling mechanisms are considered to occur subsequently. At first, the internal fouling, then the pore blockage and finally, followed by the cake formation. At the initial filtration, pore constriction is the beginning mechanism until the inside radius of pores constricts and then membrane pores incline toward blocking due to the particle aggregation until the formation of the cake layer over the blocked regions of the membrane surface.

The schematic diagram of combined three mechanism models are presented in Figure 1-b. This figure shows two main combined mechanisms which they are standard intermediate cake filtration (SIC) and standard complete cake filtration (SCC). The difference between SIC and SCC is that in SCC the particle aggregates blocks some pores while in SIC, particles enters through the pores and then pore blocking and cake filtration are happened. The five different three mechanisms, their abbreviation and final relation equations are provided in Table 1.

For development of the first model (SIC), three steps for fouling were assumed which included standard blocking, intermediate pore blockage and cake formation, respectively. The second and third models (Hagen–Poiseuille SCC and Hagen–Poiseuille SIC) also obtained by the sequential effect of pore constriction, pore blockage and cake formation mechanisms but in the basis of calculation of these models, the Hagen-poisseuille law for the flux was used. For development of the fourth and fifth models (zero-order SCC and zero-order SIC), the classical standard mechanism was modified by the assumption of the zero-order time-dependent equation for the particle

deposition inside the pores.

The modified standard blockage equation was obtained based on the assumption that portion of the particles deposit inside the pores and the pore radius constricted during the filtration process. According to the obtained results [15], the zero-order time-dependent equation was utilized for the particles deposition rate on the internal wall of pores; therefore, a new relation for the standard blocking (internal fouling) could be derived. This modified standard mechanism (zero-order standard) equation was employed instead of the classical standard mechanism to combine with the pore blockage and cake formation mechanisms to deliver two new triple mechanism models namely zero order standard-complete pore blocking-cake formation (zero-order SCC) model and zero order standard-intermediate pore blocking-cake formation (zero-order SIC) model.

Table 1
Combined three mechanisms models, abbreviations, related equations and their fitted parameters.

Entry	Model	Abbreviation	Relation	Fitted parameters
1	Standard blocking, intermediate pore blockage and cake formation	SIC	Eq. 19	α', f', R', R_{c0}, β
2	Standard blocking, complete pore blockage and cake formation (using the Hagen–Poiseuille law)	Hagen–Poiseuille SCC	Eq. 29	α, f', R', R_{c0}, α_{in}
3	Standard blocking, intermediate pore blockage and cake formation (using the Hagen–Poiseuille law)	Hagen–Poiseuille SIC	Eq. 30	α', f', R', R_{c0}, α_{in}
4	Zero order standard blocking, complete pore blockage, cake formation	Zero-order SCC	Eq. 36	α, f', R', R_{c0}, K_{s0}"
5	Zero order standard blocking, intermediate pore blockage and cake formation	Zero-order SIC	Eq. 37	α', f', R', R_{c0}, K_{s0}"

3.1. Standard blocking, intermediate pore blockage and cake formation

The volumetric flow rate through the membrane was assumed to be expressed as the sum of the flow through the unblocked (Q_{open}) and blocked pores ($Q_{blocked}$):

$$Q = Q_{open} + Q_{blocked} \tag{5}$$

The governing equation for classical standard mechanism is:

$$\frac{dA_{open}}{dt} = \frac{d(N_0 \pi r_p^2 \delta_m)}{dt} = -\alpha_{in} Q_{open} C_b \tag{6}$$

By integration, the normalized flux equation for the classical standard mechanism obtained as:

$$\frac{J_{open}}{J_0} = \frac{1}{(1+\beta Q_0 C_b t)^2} \qquad \text{where} \quad \beta = \frac{\alpha_{in}}{\pi r_p^2 \delta_m} \tag{7}$$

The classical intermediate pore blockage expression was applied to obtain the rate of pore blockage:

$$\frac{dA_{open}}{dt} = -\alpha' Q_{open} \frac{A_{open}}{A_0} C_b = -\alpha' J_{open} \frac{A_{open}^2}{A_0} C_b \tag{8}$$

This equation (Eq. 8) is the governing equation for the complete pore blockage mechanism. For accounting the pore constriction effects on the external pore blockage, Eq. 7 inserted into the Eq. 8 and the area of open pores versus the time is obtained as:

$$\frac{A_{open}}{A_0} = \left(1 - \frac{\alpha'}{\beta A_0 (1+\beta Q_0 C_b t)} + \frac{1}{\beta A_0}\right)^{-1} \tag{9}$$

Total flow rate through the open pores can be evaluated by combining Eqs. 7 and 9 as:

$$\frac{Q_{open}}{Q_0} = \frac{J_{open}}{J_0}\frac{A_{open}}{A_0} = \frac{1}{(1+\beta Q_0 C_b t)^2}\left(1 - \frac{\alpha'}{\beta A_0 (1+\beta Q_0 C_b t)} + \frac{1}{\beta A_0}\right)^{-1} \tag{10}$$

The flow rate through the blocked pores (covered area) can be evaluated as:

$$Q_{blocked} = \int_{A_{blocked}} \frac{\Delta P}{\mu (R_{m,in} + R_c)} dA \tag{11}$$

where, $R_{m,in}$ is the sum of membrane and the pore constriction resistances. R_c is the resistance caused by the cake layer formed on the membrane surface. Cake layer grows over the time interval t_c to t, therefore the pore constriction is affected by:

$$R_{m,in} = R_m (1+\beta Q_0 C_b t_c)^2 \tag{12}$$

The rate of cake formation over each blocked region of the membrane is assumed to be proportional to the movement of particles in that particular region:

$$\frac{dm_C}{dt} = f' J_{blocked} C_b \tag{13}$$

$$\frac{dR_C}{dt} = R' \frac{dm_C}{dt} = f' R' J_{blocked} C_b \tag{14}$$

where, m_c is the mass of particles deposit per unit area, and f' is the fraction of particles that contributes to the growth of the deposit, R' is the specific resistance of the cake layer and $J_{blocked}$ is the filtrate flux through each region of the membrane:

$$J_{blocked} = \frac{\Delta P}{\mu (R_{m,in} + R_c)} \tag{15}$$

The total resistance over each region of the membrane can be obtained by inserting $J_{blocked}$ from Eq. 15 in Eq. 14 and then integration:

$$R_{m,in} + R_m = \sqrt{[R_{c0} + R_m (1+\beta Q_0 C_b t_c)^2]^2 + 2\frac{f' R' \Delta P C_b}{\mu}(t - t_c)} \tag{16}$$

where, R_{c0} is the initial resistance of the deposit. The open area of the membrane decreases and is proportional to its blocked area of membrane which increases with the time; therefore, by differentiation of Eq. 9:

$$dA_{block} = -dA_{open} = \alpha' Q_0 C_b \beta^2 A_0^2 \left((1+\beta A_0)((1+\beta Q_0 C_b t_c)) - \alpha'\right)^{-2} dt_c \tag{17}$$

By substitution of Eqs. 16 and 17 into Eq. 11, the volumetric flow rate through the blocked area is obtained as:

$$\frac{Q_{blocked}}{Q_0} = \int_0^t \frac{\alpha' Q_0 C_b \beta^2 A_0 ((1+\beta A_0)((1+\beta Q_0 C_b t_c)) - \alpha')^{-2} dt_c}{\sqrt{\left[\frac{R_{c0}}{R_m} + (1+\beta Q_0 C_b t_c)^2\right]^2 + 2\frac{f' R' \Delta P C_b}{\mu R_m^2}(t - t_c)}} dt_c \tag{18}$$

Finally, the total volumetric flow rate is the summation of volume flow rates through the open and blocked pores:

$$\frac{Q}{Q_0}=\frac{1}{(1+\beta Q_0 C_b t)^2}\left(1-\frac{\alpha'}{\beta A_0(1+\beta Q_0 C_b t)}+\frac{1}{\beta A_0}\right)^{-1} \quad (19)$$

$$+\int_0^t \frac{\alpha' Q_0 C_b \beta^2 A_0((1+\beta A_0)(1+\beta Q_0 C_b t_c)-\alpha')^{-2} dt_c}{\sqrt{\left[\frac{R_{c0}}{R_m}+(1+\beta Q_0 C_b t_c)^2\right]^2+2\frac{f' R' \Delta P C_b}{\mu R_m{}^2}(t-t_c)}} dt_c$$

3.2. Standard blocking, complete pore blockage and cake formation (using the Hagen–Poiseuille law for flux)

According to the Hagen–Poiseuille law, the flow of an incompressible uniform viscous liquid through a cylindrical tube with a constant circular cross-section has the fourth order dependence on pore radius. The Hagen-Poisseuille law for the flux is:

$$J_{open}=\frac{N_0 \pi r_p^4 \Delta P}{8\mu\delta_m} \quad (20)$$

By inserting the Hagen-Poisseuille law (Eq. 20) into Eq. 6 and then integration, the pores radius as a function of time can be expressed as:

$$r_p^4=\left(\frac{N_0 \alpha_{in} \pi C_b \Delta P}{4\mu\delta_m^2} t+\frac{1}{r_{p0}^4}\right)^{-1} \quad (21)$$

The calculations are described in appendix 1 more completely. By substitution of Eq. 21 in Hagen-Poisseuille law, the flux equation can be obtained as:

$$J_{open}=\frac{N_0 \pi \Delta P}{8\mu\delta_m}\left(\frac{N_0 \alpha_{in} \pi C_b \Delta P}{4\mu\delta_m^2} t+\frac{1}{r_{p0}^4}\right)^{-1} \quad (22)$$

$$=J_0\left(1+\frac{2J_0 C_b \alpha_{in}}{\delta_m} t\right)^{-1}$$

This normalized flux equation was applied as the standard mechanism governing equation. For the complete blocking mechanism:

$$\frac{dA_{open}}{dt}=-\alpha Q_{open} C_b=-\alpha J_{open} A_{open} C_b \quad (23)$$

By inserting Eq. 22 into Eq. 23 and then integration, the area of open pores versus the time is obtained as:

$$\frac{A_{open}}{A_0}=\left(1+\frac{2J_0 C_b \alpha_{in}}{\delta_m} t\right)^{\left(\frac{-\alpha\delta_m}{2\alpha_{in}}\right)} \quad (24)$$

The volume flow rate through the open pores can be evaluated by combining Eqs. 22 and 24:

$$\frac{Q_{open}}{Q_0}=\frac{J_{open}}{J_0}\frac{A_{open}}{A_0}=\left(1+\frac{2J_0 C_b}{\delta_m} t\right)^{-\left(1+\frac{\alpha\delta_m}{2\alpha_{in}}\right)} \quad (25)$$

For the volumetric flow rate through the blocked pores, by calculation similar to the SIC model:

$$R_{m,in}+R_c=\sqrt{[R_{c0}+R_m(1+\frac{2J_0 C_b \alpha_{in}}{\delta_m} t_c)]^2+2\frac{f' R' \Delta P C_b}{\mu}(t-t_c)} \quad (26)$$

The area of blocked pores increased with time as:

$$dA_{block}=-dA_{open}=J_0 \alpha C_b A_0\left(1+\frac{2J_0 C_b \alpha_{in}}{\delta_m} t_c\right)^{-\left(1+\frac{\alpha\delta_m}{2\alpha_{in}}\right)} dt_c \quad (27)$$

The volume flow rate through the blocked pores is:

$$\frac{Q_{blocked}}{Q_0}=\int_0^t \frac{J_0 \alpha C_b\left(1+\frac{2J_0 C_b \alpha_{in}}{\delta_m} t_c\right)^{-\left(1+\frac{\alpha\delta_m}{2\alpha_{in}}\right)}}{\sqrt{\left[\frac{R_{c0}}{R_m}+(1+\frac{2J_0 C_b \alpha_{in}}{\delta_m} t_c)\right]^2+2\frac{f' R' \Delta P C_b}{\mu R_m{}^2}(t-t_c)}} dt_c \quad (28)$$

Finally, the total flow rate through the fouling membrane is calculated by the summation of the flow rate through open and blocked pores:

$$\frac{Q}{Q_0}=\left(1+\frac{2J_0 C_b \alpha_{in}}{\delta_m} t\right)^{-\left(1+\frac{\alpha\delta_m}{2\alpha_{in}}\right)} \quad (29)$$

$$+\int_0^t \frac{J_0 \alpha C_b\left(1+\frac{2J_0 C_b \alpha_{in}}{\delta_m} t_c\right)^{-\left(1+\frac{\alpha\delta_m}{2\alpha_{in}}\right)}}{\sqrt{\left[\frac{R_{c0}}{R_m}+(1+\frac{2J_0 C_b \alpha_{in}}{\delta_m} t_c)\right]^2+2\frac{f' R' \Delta P C_b}{\mu R_m{}^2}(t-t_c)}} dt_c$$

3.3. Standard blocking, intermediate pore blockage and cake formation (using the Hagen–Poiseuille law for the flux)

By similar method and using Eq. 22 in intermediate governing expression (Eq. 8), the normalized flow rate equation derived as:

$$\frac{Q}{Q_0}=\left(1+\frac{2J_0 C_b \alpha_{in}}{\delta_m} t\right)^{-1}\left(1+\frac{\alpha'\delta_m}{2\alpha_{in}}\ln\left(1+\frac{2J_0 C_b \alpha_{in}}{\delta_m} t\right)\right)^{-1} \quad (30)$$

$$+\int_0^t \frac{\alpha' J_0 C_b\left(1+\frac{2J_0 C_b \alpha_{in}}{\delta_m} t_c\right)^{-1}\left(1+\frac{\alpha'\delta_m}{2\alpha_{in}}\ln\left(1+\frac{2J_0 C_b \alpha_{in}}{\delta_m} t_c\right)\right)^{-2}}{\sqrt{\left[\frac{R_{c0}}{R_m}+(1+\frac{2J_0 C_b \alpha_{in}}{\delta_m} t_c)\right]^2+2\frac{f' R' \Delta P C_b}{\mu R_m{}^2}(t-t_c)}} dt_c$$

3.4. Zero order standard blocking, complete pore blockage, cake formation

The normalize flux equation for zero order standard mechanism was calculated according to previous work [15], as:

$$\frac{J_{open}}{J_0}=\left(\frac{r}{r_0}\right)^4=(1-K_{so}'' t)^4 \quad (31)$$

and $K_{s0}''=\frac{K_{s0}'}{r_0}$. The calculations are described in Appendix 2 more completely.

By inserting Eq. 31 into the governing equation of complete pore blockage mechanism (Eq. 23) and then integration, the open pores area is calculated as:

$$\frac{A_{open}}{A_0}=\exp\left(\frac{\alpha C_b J_0}{5K_{s0}''}\left((1-K_{s0}'' t)^5-1\right)\right) \quad (32)$$

The volumetric flow rate through the open pores is evaluated by combining Eqs. 31 and 32 as:

$$\frac{Q_{open}}{Q_0}=\frac{J_{open}}{J_0}\frac{A_{open}}{A_0} \quad (33)$$

$$=(1-K_{s0}'' t)^4 \exp\left(\frac{\alpha C_b J_0}{5K_{s0}''}\left((1-K_{s0}'' t)^5-1\right)\right)$$

The volumetric flow rate through the blocked area was calculated by the method similar to previous calculations and the results are:

$$R_{m,in}+R_c=\sqrt{[R_{c0}+R_m(1-K_{s0}'' t_c)^{-4}]^2+2\frac{f' R' \Delta P C_b}{\mu}(t-t_c)} \quad (34)$$

The volumetric flow rate through the blocked pores becomes:

$$\frac{Q_{blocked}}{Q_0} = \int_0^t \frac{\alpha C_b J_0 (1 - K''_{s0} t_c)^4 \exp\left(\frac{\alpha C_b J_0}{5K''_{s0}}((1 - K''_{s0} t_c)^5 - 1)\right)}{\sqrt{\left[\frac{R_{c0}}{R_m} + (1 - K''_{s0} t_c)^{-4}\right]^2 + 2\frac{f' R' \Delta P C_b}{\mu R_m{}^2}(t - t_c)}} dt_c \quad (35)$$

Finally, the total flow rate through the membrane is expressed as:

$$\frac{Q}{Q_0} = (1 - K''_{s0} t)^4 \exp\left(\frac{\alpha C_b J_0}{5K''_{s0}}((1 - K''_{s0} t)^5 - 1)\right) \quad (36)$$

$$+ \int_0^t \frac{\alpha C_b J_0 (1 - K''_{s0} t_c)^4 \exp\left(\frac{\alpha C_b J_0}{5K''_{s0}}((1 - K''_{s0} t_c)^5 - 1)\right)}{\sqrt{\left[\frac{R_{c0}}{R_m} + (1 - K''_{s0} t_c)^{-4}\right]^2 + 2\frac{f' R' \Delta P C_b}{\mu R_m{}^2}(t - t_c)}} dt_c$$

3.5. Zero order standard blocking, intermediate pore blockage and cake formation

By similar method and using Eq. 31 in intermediate governing expression (Eq. 8), the normalized flow rate equation is derived as:

$$\frac{Q}{Q_0} = (1 - K''_{s0} t)^4 \left(1 - \frac{\alpha' C_b J_0}{5K''_{s0}}((1 - K''_{s0} t)^5 - 1)\right)^{-1} \quad (37)$$

$$+ \int_0^t \frac{\alpha' C_b J_0 (1 - K''_{s0} t_c)^4 \left(1 - \frac{\alpha' C_b J_0}{5K''_{s0}}\left((1 - K''_{s0} t_c)^5 - 1\right)\right)^{-2}}{\sqrt{\left[\frac{R_{c0}}{R_m} + (1 - K''_{s0} t_c)^{-4}\right]^2 + 2\frac{f' R' \Delta P C_b}{\mu R_m{}^2}(t - t_c)}} dt_c$$

4. Materials and methods

4.1. Materials

BSA solution as filtration liquid was prepared by dissolving the BSA powder (Merck Millipore) in water. The BSA solutions were filtered through the 0.2 µm hydrophilic polycarbonate track etched (PCTE) membrane (GTTP02500, Isopore Membrane Filter, Merck Millipore, 25 mm diameter). The membrane surface area was 4×10^{-5} m^2.

4.2. Filtration experiments

BSA solutions with concentrations of 1, 2, 4, and 8 g/L were prepared. A constant transmembrane pressure of 14 kPa was applied for combined three mechanism experiments. The filtrations were performed without stirring. The volumetric flow rates were measured versus the time and by using a digital balance (Sartorious Model 1580). The flow rate was measured during the filtration for 2 hours. All experiments were performed at room temperature (around 20 °C).

For investigation of the classical models, the total filtrate volume (m^3) was measured. The BSA solution with the concentration of 2 g/L at 69 kPa pressure was filtered and the filtrate was collected during 35 min filtration at 20 °C (±5).

4.3. Operating parameters

The proposed combined models have been driven at constant pressure. Therefore, transmembrane pressure (TMP) was considered to be set at 69 kPa based on the type of membrane (0.2 µm track-etched MF). The experiments were performed at room temperature (20±5 °C). The BSA concentrations were changed from low (1 g/L) to high (8 g/L) at four levels. The pH was set at 7; higher than the BSA isoelectric point (~5) [15].

5. Results and discussion

The best fit parameters were obtained by minimizing the sum of squared residuals between the model and the experimental data. For the consistency of model with the experimental data, some square error (SSE) was calculated for each model and the results are presented for comparison of the models.

5.1. Classical models

The results of modeling the experimental total filtrate volume for the BSA solution filtration in the concentration of 2 g/L for the classical models (standard blocking, complete blocking, intermediate blocking and cake filtration) are presented in Figure 2. Table 2 shows the fit constant parameters and their calculated SEE. At the beginning of the time, the complete, standard and intermediate blocking models could predict the experimental data well. This result shows that some BSA monomers or oligomers could enter the membrane pores [14], but some else may form aggregates and block some pores of membrane [15].

The complete blocking model fits the data at moderate time, but could not predict the experimental data at longer times. This result represent that the complicated phenomenon has been happened especially for longer times. The cake formation mechanism could not predict the experimental especially at the beginning and moderate time. The cake formation model fitted the data around 1400 s and demonstrated that this time the layer deposition may be occurred [24].

The SEE for the standard blocking, complete blocking, intermediate blocking and cake filtration are 3.77×10^{-1}, 9.11×10^{-5}, 4.23×10^{-4} and 5.71×10^{-3}, respectively. The comparison between the SEE for the four classical mechanisms reveals that the standard blocking cannot predict the experimental data at whole time. In other words, this result show that particles could not enter the membrane frequently due to the high BSA particle aggregate [15]. Table 2 also compares the fit parameters with Bolton et al. [8]. They have obtained the data for 2.5 g/L BSA filtered through Viresolve 180 membrane at 207 kPa. There are significant differences between Bolton and co-workers' classic fit parameters and current study, except for K_b. The source of this difference may be due to being difference in the type of applied membrane or TMP.

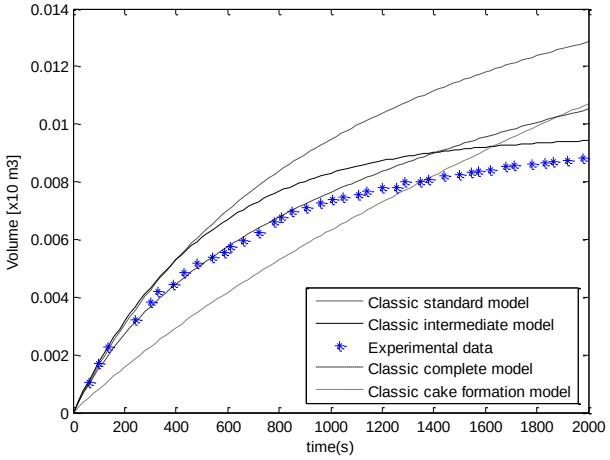

Fig. 2. Total filtrate volume (m^3) experimental data and classical models for BSA solution filtration with the concentration of 2 g/L at 69 kPa and 20 °C (±5).

Table 2
Fitted parameter values for the classical models. BSA solution concentration was 2 g/L at 69 kPa and 20 °C (±5).

Model	Fit parameter	SEE	Bolton et al. [8]*
Standard blocking	$K_s = 100\ m^{-1}$	3.77×10^{-1}	$K_s = 13.2\ m^{-1}$
Complete blocking	$K_b = 2.0\times10^{-3}\ s^{-1}$	9.11×10^{-5}	$K_b = 2.61\times10^{-3}\ s^{-1}$
Intermediate blocking	$K_i = 2.6\times10^{3}\ m^{-1}$	4.23×10^{-4}	$K_i = 30.5\ m^{-1}$
Cake formation	$K_c = 6\times10^{6}\ s/m^2$	5.71×10^{-3}	$K_c = 7.21\times10^{5}\ s/m^2$

* Data for 2.5 g/L BSA filtered through Viresolve 180 membrane at 207 kPa

5.2. Combined three mechanisms models

The Q_0 was measured and its value for different feed concentrations was between 1.3×10^{-7} to 1.6×10^{-7} m^3/s. The R_m value for the clean membrane by measuring the flux of passing distilled water thought the membrane at 14 kPa was 1.75×10^{10} m^{-1}.

The experimental data for the constant pressure filtration of four different BSA solutions (concentrations varying from 1 to 8 g/L) and the model predictions for the combined sequential effects of three different classical fouling mechanisms are shown in Figures 3-7. These figures show the normalized volumetric flow rate (Q/Q_0) as a function of the filtration time. Solid curves represent the models calculations based on the best fit parameters.

The normalized flow rate versus the time for the experimental data and the model predictions for the SIC (Eq. 19) is shown in Figure 3. The normalized flow rate declines more rapidly with increasing the BSA concentration.

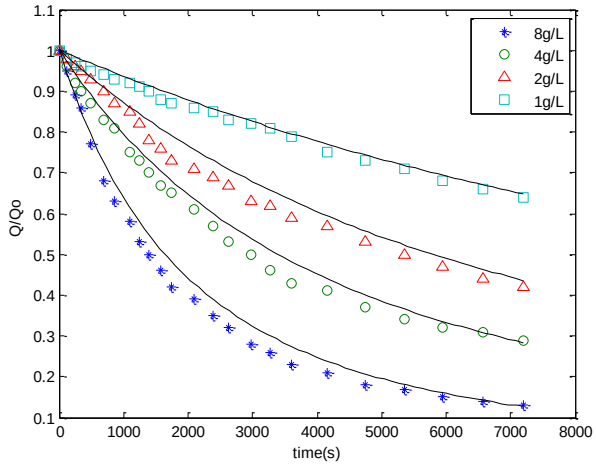

Fig. 3. Normalized flow rate experimental data for BSA solutions filtration (14 kPa and 20°C (±5)) and the predictions (solid curves) using combined standard blocking-intermediate pore blockage-cake formation model at different feed concentrations.

At the beginning of the filtration, the flux decreases rapidly, when the pore blockage mechanism is dominant, and then it declines gradually during the filtration, when the fouling is dominated by the cake filtration. The filtrate flow rate for higher BSA concentrations declined more rapidly. The flow rate versus time curves at low BSA concentrations (1 and 2 g/L) are relatively linear [24]. This behavior is likely due to the fact that fouling occurs through a combination of different fouling mechanisms. In these cases, the flow rate diagram versus the time does not give a clear indication of the dominant fouling mechanism. At higher concentration (8 g/L), the data shows changes in the concave from the initial to the final of the filtration. This result indicates that the fouling is mainly caused by pore blockage during the early stage of filtration and dominated by cake filtration at long filtration times. R' is the specific protein layer resistance, which is assumed to be constant during a constant pressure filtration and f' is the fraction of the proteins that cause the buildup of the cake layer [14]. In this combined model, α', β, $f'R'$ represent the parameters for pore blockage, pore constriction, and cake filtration, R_{c0} is the initial resistance of one single protein aggregate, respectively.

The model predictions and experimental data have rather good agreements, but there is some discrepancy between the data and the model. The fit parameters for the SIC model are shown in Table 3. The model parameters were calculated by curve fitting the experimental data and provided by Matlab software. This table also shows the SSE and results show that their SSE is in the order of 10^{-7} for different concentrations.

The second triple-mechanism model applied to filtration of BSA solution is the Hagen–Poiseuille SCC. The normalized filtrate flow rate data and the model predictions (Eq. 29) are shown in Figure 4. At the extended time, the flux does not significantly change with the time and the concentration of solution. The transition between these two stages, the pore blockage and cake filtration, is determined by the change in slope of the flux with the time [10].

Table 3
SIC fouling model parameters and the SEE for the best fit.

C_b (g/L)	α '	f 'R'	R_{C0}	β	SSE
1	0.972	15.11×10^{13}	29.71×10^{10}	200.0	3.11×10^{-7}
2	0.975	15.16×10^{13}	29.75×10^{10}	198.0	6.53×10^{-7}
4	0.980	15.19×10^{13}	29.90×10^{10}	197.0	7.92×10^{-7}
8	0.999	15.23×10^{13}	30.00×10^{10}	195.7	8.01×10^{-7}

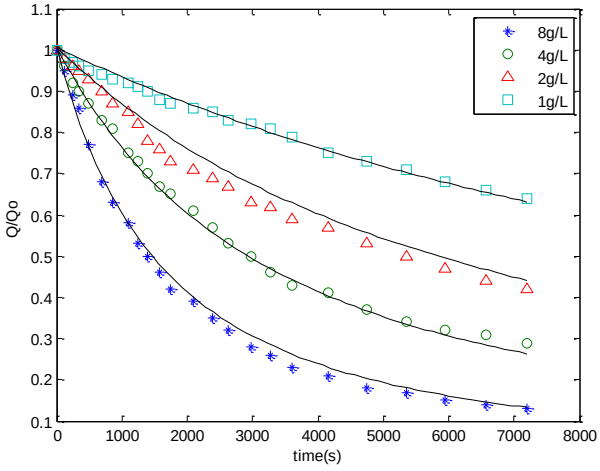

Fig. 4. Normalized flow rate experimental data for BSA solutions filtration (14 kPa and 20°C (±5)) and the predictions (solid curves) using combined standard blocking-complete pore blockage-cake formation (using the Hagen-Poisseuille law for flux) model at different feed concentrations.

The fit parameters for the Hagen–Poiseuille SCC model and the SSE are shown in Table 4. The SSE results for the model consistency are in the order of 10^{-8} for different concentrations.

Table 4
Hagen–Poiseuille SCC fouling model parameters and the SEE for the best fit.

C_b (g/L)	α	f 'R'	R_{C0}	α_{in}	SEE
1	0.0637	17.25×10^{13}	17.94×10^{10}	2.344×10^{-8}	2.64×10^{-8}
2	0.0639	17.40×10^{13}	17.95×10^{10}	2.326×10^{-8}	3.25×10^{-8}
4	0.0640	17.50×10^{13}	17.97×10^{10}	2.312×10^{-8}	3.79×10^{-8}
8	0.0641	18.00×10^{13}	18.00×10^{10}	2.300×10^{-8}	4.11×10^{-8}

The third triple-mechanism model applied to the filtration of BSA solution is the Hagen–Poiseuille SIC. The normalized filtrate flow rate data and the model predictions (Eq. 30) are shown in Figure 5. Both external (intermediate) and internal (standard) blocking appear at the beginning of fouling, whereas internal blocking disappears for the subsequent steps of the process [18].

Table 5 shows the fit parameters for the Hagen–Poiseuille SIC model and the SSE. The SSE results for the model consistency are in the order of 10^{-8} for different concentrations.

The fourth triple-mechanism model applied to the filtration of BSA solution is the zero-order SCC. Figure 6 represents the normalized filtrate flow rate data and the model predictions (Eq. 36).

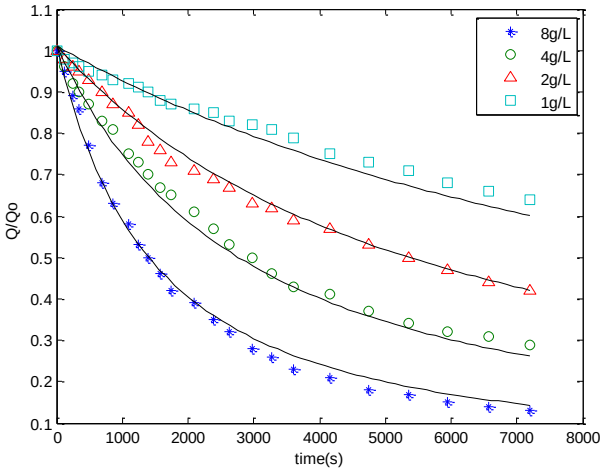

Fig. 5. Normalized flow rate experimental data for BSA solutions filtration (14 kPa and 20°C (±5)) and the predictions (solid curves) using combined standard blocking-intermediate pore blockage-cake formation (using Hagen-Poisseuille law for flux) model at different feed concentrations.

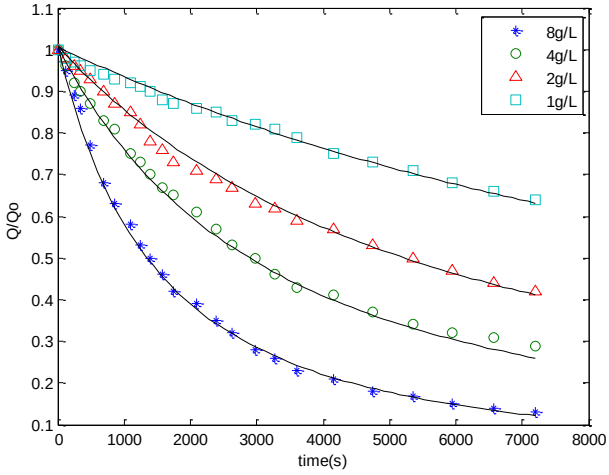

Fig. 6. Normalized flow rate experimental data for BSA solutions filtration (14 kPa and 20°C (± 5)) and the predictions (solid curves) using zero order standard blocking, complete pore blockage, cake formation model at different feed concentrations.

Table 6 illustrates the fit parameters for the zero-order SCC model and the SSE. The SSE results for the model consistency are in the order of 10^{-10} and this model predicts the experimental data more accurately rather than three prior combined mechanisms.

The fifth triple-mechanism model applied to the filtration of BSA solution is the zero-order SIC. Figure 7 displays the normalized filtrate flow rate data for the BSA solution filtration and the model predictions (Eq. 37).

Table 7 represents the fit parameters for zero-order SIC model and the SSE. The SSE results for the model consistency are in the order of 10^{-10} and therefore, this model similar to the fourth model, predicts the experimental data well.

Table 5
Hagen–Poiseuille SIC fouling model parameters and the SEE for the best fit.

C_b (g/L)	α'	f 'R'	R_{C0}	α_{in}	SEE
1	0.0860	16.21×10^{13}	34.71×10^{10}	2.53×10^{-8}	3.77×10^{-8}
2	0.0868	16.22×10^{13}	34.83×10^{10}	2.47×10^{-8}	3.21×10^{-8}
4	0.0870	16.25×10^{13}	34.95×10^{10}	2.33×10^{-8}	3.88×10^{-8}
8	0.0875	16.29×10^{13}	35.00×10^{10}	2.26×10^{-8}	4.09×10^{-8}

Table 6
Zero-order SCC fouling model parameters and the SEE for the best fit.

C_b (g/L)	α	f 'R'	R_{C0}	K_{s0}''	SEE
1	1.20	16.01×10^{13}	32.11×10^{10}	3.62×10^{-4}	6.12×10^{-10}
2	1.25	16.13×10^{13}	32.46×10^{10}	3.41×10^{-4}	6.15×10^{-10}
4	1.28	16.21×10^{13}	32.73×10^{10}	3.33×10^{-4}	6.35×10^{-10}
8	1.35	16.27×10^{13}	32.84×10^{10}	3.21×10^{-4}	6.32×10^{-10}

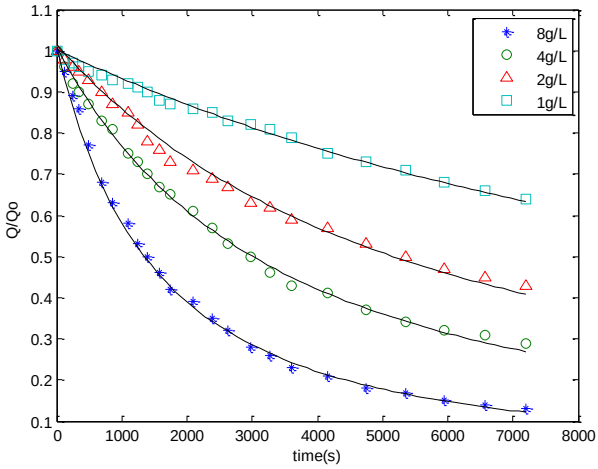

Fig. 7. Normalized flow rate experimental data for BSA solutions filtration (14 kPa and 20°C (± 5)) and the predictions (solid curves) using zero order standard blocking, intermediate pore blockage and cake formation model at different feed concentrations.

Table 7
Zero-order SIC fouling model parameters and the SEE for the best fit.

C_b (g/L)	α'	f 'R'	R_{C0}	K_{s0}''	SEE
1	1.03	16.36×10^{13}	33.05×10^{10}	5.85×10^{-4}	6.11×10^{-10}
2	1.09	16.44×10^{13}	33.27×10^{10}	5.66×10^{-4}	6.40×10^{-10}
4	1.18	16.57×10^{13}	33.46×10^{10}	5.51×10^{-4}	6.35×10^{-10}
8	1.22	16.64×10^{13}	33.72×10^{10}	5.32×10^{-4}	6.23×10^{-10}

The values of pore blockage parameters (α' and α), for higher BSA solution concentration (8 g/L) was bigger than low concentrations (1 and 2 g/L). This fact may be due to the formation of particle aggregates in the higher concentration (8 g/L) and these aggregates may contribute to pore blockage [27].

The values of pore constriction parameters (β, α_{in} and K_{s0}'') have been decreased as the concentration increased in all models fittings. These results indicate that in high solution concentrations, the aggregate formation over the membrane surface may create some blockage and prevents smaller particles from passing through the pores [14] and accordingly, the particles are adsorbed on the pore walls; therefore, in low concentration solutions, the internal fouling occurs more than higher concentration.

The values of $f'R'$ for the lower BSA solution concentrations are smaller compared to the higher concentrations due to the fact that the fouling layer is formed mainly by the protein aggregates in higher solution concentrations [27]. This consequence also explains the higher values of R_{C0} in high concentration solutions.

Table 8 represents the comparison of current study fit parameters with the other combined models in the literature. The brought fit parameters for current research are the average in the concentrations of 1 to 8 g/L. In this table, the value of pore blockage parameter (α, α') is in the range of 1-3.5 m^2/kg, although in Ye et al. [19], α is very large due to the different feed used (alginate). The value of $f'R'$ in Duclos-Orsello at al. [14] and Zydney and Ho

[25] is in the order 10^{10} at 14 kPa TMP, but in Seifollahy Astaraee et al. [24] and current research this value is in the order of 10^{13} at higher TMP. The values of β and R_{co} are in the ranges of data reported in the literature.

6. Conclusions

In this study, BSA solutions with concentrations of 1, 2, 4, and 8 g/L were filtered through the 0.2 µm hydrophilic polycarbonate track etched membrane and the fouling behavior was investigated and modeled. The best fit parameters were obtained by minimizing the sum of squared residuals between the model and the experimental data. For the consistency of the model with the experimental data, the SSE was calculated and compared for the models.

The results showed that modeling the total filtrate volume for the BSA solution filtration in the concentration of 2 g/L by the classical models (standard blocking, complete blocking, intermediate blocking and cake filtration) the classical models could not predict the experimental precisely. The SEE for the standard blocking, complete blocking, intermediate blocking and cake filtration are 3.77×10^{-1}, 9.11×10^{-5}, 4.23×10^{-4} and 5.71×10^{-3}, respectively. These results show that the membrane fouling during BSA solution microfiltration is happened by a complicated mechanism rather than an individual mechanism.

For combined three mechanisms models, the classic standard expression has been used to describe the effect of internal fouling and then combined with other mechanisms to deliver triple-mechanism fouling models (SIC, Hagen–Poiseuille SCC and Hagen–Poiseuille SIC models). The zero-order SCC and zero-order SIC models have been obtained based on the combination of modified expression for the standard blockage [26] with other classical mechanisms. As a result, the zero-order SCC and zero-order SIC models (with the SEE in order of 10^{-10}) compared with the SIC (SSE in the order of 10^{-7}), Hagen–Poiseuille SCC and Hagen–Poiseuille SIC (SSE in the order of 10^{-8}) provide well consistency with the experimental filtrate flow rate.

Table 8
Comparison of current study average fit parameters with the other combined models in the literature.

Feed/Concentration (g/L)	Membrane type	TMP (kPa)		Fit parameters	Ref.
BSA/1-8	0.22 µm GVHP	14		α=1.08 m^2/kg β=127.6 kg f'R'=6.98×10^{10} m/kg	[14]
BSA/1-8	0.22 µm GVWP	14		α =2.88 m^2/kg β=0.864 kg f'R'=1.89×10^{10} m/kg	[14]
Alginate/50	0.22 µm TE	15-25		α= 6284 m^2/kg R_{c0}= 1×10^{10} m^{-1}	[19]
BSA/0.5-5	0.2 µm PCTE	40		α=3.50 m^2/kg R_{c0}=41.8×10^{10} m^{-1} f'R'= 5.51×10^{13} m/kg	[24]
BSA/0.4	0.2 µm PCTE	14		β=0.81 m^{-1} R_{co}=40×10^{10} m^{-1}	[25]
BSA/1-8	0.2 µm PCTE	69	SIC	α'=0.982 m^2/kg f'R'=60.69×10^{13} m/kg R_{c0}=29.84×10^{10} m^{-1} β=197.8 kg	This study
			Hagen–Poiseuille SCC	α=0.208 m^2/kg f'R'=17.54×10^{13} m/kg R_{c0}=17.96×10^{10} m^{-1} α_{in}=2.32×10^{-8} m^2/kg	
			Hagen–Poiseuille SIC	α'=0.0868 m^2/kg f'R'=16.24×10^{13} m/kg R_{c0}=34.87×10^{10} m^{-1} α_{in}=2.40×10^{-8} m^2/kg	
			Zero-order SCC	α=1.26 m^2/kg f'R'=16.16×10^{13} m/kg R_{c0}=32.44×10^{10} m^{-1} K_{s0}"=3.39×10^{-4} s^{-1}	
			Zero-order SIC	α'=1.13 m^2/kg f'R'=16.50×10^{13} m/kg R_{c0}=33.38×10^{10} m^{-1} K_{s0}"=5.58×10^{-4} s^{-1}	

Nomenclatures

A	Area of membrane (m^2)
$A_{blocked}$	Area of membrane blocked by foulant (m^2)
A_{open}	Area of unblocked membrane (m^2)
A_0	Initial area of clean membrane (m^2)
C_b	Solute bulk concentration (g L^{-1})
f′	Fractional amount of total foulant contributing to deposit growth
$J_{blocked}$	Filtrate flux within the blocked area (m s^{-1})
J_{open}	Filtrate flux within the unblocked area (m s^{-1})
J_0	Initial filtrate flux of clean membrane (m s^{-1})
K_b	Complete blocking constant (s^{-1})
K_c	Cake filtration constant (sm^{-2})
K_i	Intermediate blocking constant (m^{-1})
K_s	Standard blocking constant (m^{-1})
K_{s0}'	Adsorption blocking constant (m s^{-1})
K_{s0}"	Adsorption blocking constant, (s^{-1})
n	Cake compressibility index, dimensionless
N_0	Number of pores per membrane unit area (m^{-2})
Q	Total volumetric flow rate (m^3 s^{-1})
$Q_{blocked}$	Volumetric flow rate within the blocked area (m^3 s^{-1})
Q_{open}	Volumetric flow rate within the unblocked area (m^3 s^{-1})
Q_0	Initial volumetric flow rate of clean membrane (m^3 s^{-1})
r_p	Radius of membrane pore (m)
$R_{m,in}$	Sum of membrane and pore constriction resistances (m^{-1})

R_m	Hydraulic membrane resistance (m^{-1})
R_c	Resistance of the cake (deposit) (m^{-1})
R_{c0}	Initial resistance of the cake (deposit) (m^{-1})
R'	Specific protein layer resistance (m kg^{-1})
t	Filtration time (s)
t_c	Characteristic time for initial cake formation (s)
V	Total filtrate volume per area (m^3m^{-2})
V_{in}	Deposited foulant volume (m^3)

Greek symbols

ΔP	Transmembrane pressure (N m^{-2})
α	Complete pore blockage parameter (m^2 kg^{-1})
α'	Intermediate pore blockage parameter (m^2 kg^{-1})
α_{in}	Internal pore blockage parameter (m^2 kg^{-1})
β	Pore constriction parameter (kg)
δ_m	Membrane thickness (m)
μ	Solution viscosity (kg m^{-1} s^{-1})

Abbreviations

BSA	Bovine serum albumin
PCTE	Polycarbonate track etched
SCC	Standard blocking, complete pore blockage and cake formation
SIC	Standard blocking, intermediate pore blockage and cake formation
SSE	Sum square error
TE	Track etched
TMP	Transmembrane pressure

Appendix 1

$$\frac{dA_{open}}{dt} = \frac{d\left(N_0 \pi r_p^2 \delta_m\right)}{dt} = -\alpha_{in} Q_{open} C_b = -\alpha_{in} J_{open} A_{open} C_b$$

$$\Rightarrow 2N_0 \pi \delta_m r_p dr_p = -\alpha_{in} Q_{open} C_b = -\alpha_{in}\left(\frac{N_0 \pi r_p^4 \Delta P}{8\mu\delta_m}\right)\left(N_0 \pi r_p^2\right) C_b dt$$

$$\Rightarrow 16\frac{dr_p}{r_p^5} = -\frac{\alpha_{in} N_0 \pi \Delta P C_b}{\mu \delta_m^2} dt \xrightarrow{Integration} -4r_p^{-4}\Big|_{r_{p0}}^{r_p} = -\frac{\alpha_{in} N_0 \pi \Delta P C_b}{\mu \delta_m^2} t\Big|_0^t$$

$$\Rightarrow \left(\frac{1}{r_p^4} - \frac{1}{r_{p0}^4}\right) = \frac{N_0 \alpha_{in} \pi C_b \Delta P}{4\mu\delta_m^2} t \Rightarrow r_p^4 = \left(\frac{N_0 \alpha_{in} \pi C_b \Delta P}{4\mu\delta_m^2} t + \frac{1}{r_{p0}^4}\right)^{-1}$$

Appendix 2

In the previous combination of classical mechanisms, the pore constriction mechanism equation had been derived by assuming that all of particles contribute in the internal fouling and then that equation combined with other classical mechanisms, but in this study the modified standard blockage equation was obtained by the assumption that only some portion of particles deposit inside the pore walls and some else may supply to the pore blockage or cake filtration. The zero order time-dependent equation was utilized for the kinetic of particles deposition rate on the internal wall of pores. For this kinetics, calculations are continued so:

$$\frac{dV_{in}}{dt} = K'_{s0} A; A = 2\pi r \delta_m; V_{in} = \pi(r_0^2 - r^2)\delta_m$$

Consequently,

$$r = r_0 - K'_{s0} t$$

According to Hagen–Poiseuille law the increase in the resistance is related to the filtration time as:

$$\frac{J_{open}}{J_0} = \left(\frac{r}{r_0}\right)^4 = (1 - K''_{so} t)^4; K''_{s0} = \frac{K'_{so}}{r_0}$$

References

[1] R.W. Field, D. Wu, J.A. Howell, B.B. Gupta, Critical flux concept for microfiltration fouling, J. Membr. Sci. 100 (1995) 259–279.

[2] W.-M. Lu, C.-C. Lai, K.-J. Hwang, Constant pressure filtration of submicron particles, Sep. Technol. 5 (1995) 45–53.

[3] K. Stamatakis, C. Tien, Cake formation and growth in cake filtration, Chem. Eng. Sci. 46 (1991) 1917-1933.

[4] K.-J. Hwang, C.-Y Liao, K.-L. Tung, Analysis of particle fouling during microfiltration by use of blocking models, J. Membr. Sci. 287 (2007) 287–293.

[5] C.-C. Ho, A.L. Zydney, Effect of membrane morphology on the initial rate of protein fouling during microfiltration, J. Membr. Sci. 155 (1999) 261–275.

[6] K.-J. Hwang, T.-T. Lin, Effect of morphology of polymeric membrane on the performance of cross- flow microfiltration, J. Membr. Sci. 199 (2002) 41–52.

[7] E. Iritani, N. Katagiri, Y. Sugiyama, K. Yagishita, Analysis of flux decline behaviors in filtration of very dilute suspensions, AIChE J. 53 (2007) 2275–2283.

[8] G. Bolton, D. LaCasse, R. Kuriyel, Combined models of membrane fouling: Development and application to microfiltration and ultrafiltration of biological fluids, J. Membr. Sci. 277 (2006) 75–84.

[9] E.M. Tracey, R.H. Davis, Protein fouling of track-etched polycarbonate microfiltration membranes, J. Colloid Interface Sci. 167 (1994) 104–116.

[10] C.-C. Ho, A.L. Zydney, A combined pore blockage and cake filtration model for protein fouling during microfiltration, J. Colloid. Interface. Sci. 232 (2000) 389–399.

[11] W. Yuan, A. Kocic, A.L. Zydney, Analysis of humic acid fouling during microfiltration using a pore blockage–cake filtration model, J. Membr. Sci. 198 (2002) 51–62.

[12] M. Taniguchi, J.E. Kilduff, G. Belfort, Modes of natural organic matter fouling during ultrafiltration, Environ. Sci. Technol. 37 (2003) 1676–1683.

[13] A. Cassano, M. Marcia, E. Drioli, Clarification of blood orange juice by ultrafiltration: analyses of operating parameters, membrane fouling and juice quality, Desalination. 212 (2007) 15–27.

[14] C. Duclos-Orsello, W. Li, C.-C. Ho, A three mechanism model to describe fouling of microfiltration membranes, J. Membr. Sci. 280 (2006) 856–866.

[15] K. Nakamura, K. Matsumoto, Adsorption behavior of BSA in microfiltration with porous glass membrane, J. Membr. Sci. 145 (1998) 119–128.

[16] W.R. Bowen, J.I. Calvo, A. Hernandez, Steps of membrane blocking in flux decline during protein microfiltration, J. Membr. Sci. 101 (1995) 153–165.

[17] K. Xiao, X. Wang, X. Huang, T.D. Waite, X. Wen, Combined effect of membrane and foulant hydrophobicity and surface charge on adsorptive fouling during microfiltration, J. Membr. Sci. 373 (2011) 140–151.

[18] J. Jacob, P. Pradanos, J.I. Calvo, A. Hernandez, G. Jonsson, Fouling kinetics and associated dynamics of structural modifications, Colloids. Surf. A Physicochem. Eng. 138 (1998) 173–183.

[19] Y. Ye, P. Le Clech, V. Chen, A.G. Fane, B. Jefferson, Fouling mechanisms of alginate solutions as model extracellular polymeric substances, Desalination. 175 (2005) 7–20.

[20] L. Hou, Z. Wang, P. Song, A precise combined complete blocking and cake filtration model for describing the flux variation in membrane filtration process with BSA solution, J. Membr. Sci. 542 (2017) 186–194.

[21] M. Yao, K. Zhang, L. Cui, Characterization of protein–polysaccharide ratios on membrane fouling, Desalination. 259 (2010) 11–16.

[22] K.-J. Hwang, P.-Y. Sz, Effect of membrane pore size on the performance of cross-flow microfiltration of BSA/dextran mixtures, J. Membr. Sci. 378 (2011) 272–279.

[23] L. Palacio, C.-C. Ho, P. Pradanos, A. Hernandez, A.L. Zydney, Fouling with protein mixtures in microfiltration: BSA–lysozyme and BSA–pepsin, J. Membr. Sci. 222 (2003) 41–51.

[24] R. Seifollahy Astaraee, T. Mohammadi, N. Kasiri, Analysis of BSA, dextran and humic acid foulingduring microfiltration, experimental and modeling, Food. Bioprod. Process. 94 (2015) 331–341.

[25] A.L. Zydney, C.-C. Ho, Scale-up of microfiltration systems: fouling phenomena and V_{max} analysis, Desalination. 146 (2002) 75–81.

[26] H. Koonani, Modeling of fouling phenomenon in microfiltration membranes, M.Sc. Thesis, Razi University, Jan. 2015.

[27] M. Meireles, P. Aimar, V. Sanchez, Albumin denaturation during ultrafiltration: Effects of operating conditions and consequences on membrane fouling, Biotechnol. Bioeng. 38 (1991) 528–534.